

Remarkably low affinity of CD4/peptide-major histocompatibility complex class II protein interactions

Peter Jönsson^{a,b,1}, Jennifer H. Southcombe^{c,d,e,1}, Ana Mafalda Santos^{c,d}, Jiandong Huo^{c,d}, Ricardo A. Fernandes^{c,d}, James McColl^a, Melissa Lever^f, Edward J. Evans^{c,d}, Alexander Hudson^{c,d}, Veronica T. Chang^{c,d}, Tomáš Hanke^c, Andrew Godkin^g, Paul D. Dunne^a, Mathew H. Horrocks^a, Matthieu Palayret^a, Gavin R. Screaton^c, Jan Petersen^{h,i}, Jamie Rossjohn^{g,h,i}, Lars Fugger^{c,d,j}, Omer Dushek^f, Xiao-Ning Xu^{c,2}, Simon J. Davis^{c,d,2}, and David Klenerman^{a,2}

^aDepartment of Chemistry, University of Cambridge, Cambridge CB2 1EW, United Kingdom; ^bDepartment of Chemistry, Lund University, SE-22100 Lund, Sweden; ^cMRC Human Immunology Unit, University of Oxford, Oxford OX3 9DS, United Kingdom; ^dWeatherall Institute of Molecular Medicine, University of Oxford, Oxford OX3 9DS, United Kingdom; ^eNuffield Department of Obstetrics and Gynaecology, University of Oxford, Oxford OX3 9DU, United Kingdom; ^fSir William Dunn School of Pathology, University of Oxford, Oxford OX1 3RE, United Kingdom; ^gDepartment of Infection and Immunity, School of Medicine, Cardiff University, Cardiff CF14 4XN, United Kingdom; ^hInfection and Immunity Program and Department of Biochemistry and Molecular Biology, Biomedicine Discovery Institute, Monash University, Clayton, VIC 3800, Australia; ⁱAustralian Research Council Centre of Excellence in Advanced Molecular Imaging, Monash University, Clayton, VIC 3800, Australia; and ^jNuffield Department of Clinical Neurosciences, Division of Clinical Neurology, University of Oxford, Oxford OX3 9DS, United Kingdom

Edited by Mark M. Davis, Stanford University, Stanford, CA, and approved March 23, 2016 (received for review July 15, 2015)

The $\alpha\beta$ T-cell coreceptor CD4 enhances immune responses more than 1 million-fold in some assays, and yet the affinity of CD4 for its ligand, peptide-major histocompatibility class II (pMHC II) on antigen-presenting cells, is so weak that it was previously unquantifiable. Here, we report that a soluble form of CD4 failed to bind detectably to pMHC II in surface plasmon resonance-based assays, establishing a new upper limit for the solution affinity at 2.5 mM. However, when presented multivalently on magnetic beads, soluble CD4 bound pMHC II-expressing B cells, confirming that it is active and allowing mapping of the native coreceptor binding site on pMHC II. Whereas binding was undetectable in solution, the affinity of the CD4/pMHC II interaction could be measured in 2D using CD4- and adhesion molecule-functionalized, supported lipid bilayers, yielding a 2D K_d of $\sim 5,000$ molecules/ μm^2 . This value is two to three orders of magnitude higher than previously measured 2D K_d values for interacting leukocyte surface proteins. Calculations indicated, however, that CD4/pMHC II binding would increase rates of T-cell receptor (TCR) complex phosphorylation by threefold via the recruitment of Lck, with only a small, 2–20% increase in the effective affinity of the TCR for pMHC II. The affinity of CD4/pMHC II therefore seems to be set at a value that increases T-cell sensitivity by enhancing phosphorylation, without compromising ligand discrimination.

protein interactions | TCR phosphorylation | adhesion | T-cell activation | binding equilibrium and kinetics

T cells with $\alpha\beta$ T-cell receptors (TCRs) comprise functionally distinct subsets depending on which transcription factors and which of two coreceptors, CD8 or CD4, they express. CD8⁺ T cells respond to peptide agonists presented by major histocompatibility class I molecules (pMHC I) and are cytotoxic, whereas conventional CD4⁺ cells recognize peptide-MHC class II (pMHC II) and provide “help” defined by the cytokines they secrete (1). Cell adhesion assays explain this functionality insofar as CD8 and CD4 bind directly to pMHC I and pMHC II, respectively (2, 3). CD4 comprises two pairs of V-set and C2-set Ig superfamily domains, with early mutational data showing that the “top” two domains bind pMHC II (4). Crystal structures of cross-species and affinity-matured CD4/pMHC II complexes suggest that CD4 binds a pocket formed by the $\alpha 2$ and $\beta 2$ domains of pMHC II (5, 6). The role of coreceptors in heightening T-cell responses is well established. For example, whereas CD4⁺ T-cells can respond to single pMHC II complexes presented by antigen-presenting cells (APCs), 30 or more complexes are required if CD4 is blocked (7).

How CD4 achieves these effects, however, is incompletely understood. Coreceptors are pivotal in recruiting the kinase Lck to TCR/pMHC complexes (8, 9), but for reasons that are unclear

coreceptor/pMHC interactions are extraordinarily weak. Traditionally, weak protein interactions are characterized using surface plasmon resonance (SPR) measurements, where one protein is tethered to the sensor surface and over it the other is passed at various concentrations. The SPR-based affinity of CD8 for pMHC I is 50–200 μM (10). However, SPR has thus far failed to detect interactions between CD4 and pMHC II, setting a lower limit of the K_d at least two orders of magnitude higher than for typical interacting leukocyte-expressed proteins (5, 10, 11).

Here, we use SPR assays to extend the upper limit of the CD4/pMHC II solution affinity. However, the interactions of proteins in solution may differ from those at contacts between two cells, or between a cell surface and model lipid bilayer (11–14). We therefore also analyzed the 2D affinity of the CD4/pMHC II interaction for B cells interacting with supported lipid bilayers (SLBs) containing fluorescently labeled CD4 and the small T-cell adhesion protein CD2, used to create a physiological context for CD4/pMHC II binding. CD2 is expressed by T cells and binds CD58 on B cells with much higher affinity than the CD4/pMHC II interaction (15, 16). Including CD2 ensured that CD4/pMHC II

Significance

The function of the T-cell coreceptor CD4 presents a long-standing puzzle. Although it is among the most potent modulators of immune responses, CD4 interacts with its binding partner, peptide-major histocompatibility class II (pMHC II), with previously unmeasurably low affinity. Here, we set a new upper limit for the solution affinity of CD4 and pMHC II and show that the two-dimensional dissociation constant in supported lipid bilayers is as much as two to three orders of magnitude higher than that for other interacting leukocyte surface proteins. These findings extend the known physical limits of functional protein interactions at the cell surface and suggest new ways that T cells may use differential receptor affinities during antigen recognition and discrimination.

Author contributions: P.J., J.H.S., G.R.S., O.D., X.-N.X., S.J.D., and D.K. designed research; P.J., J.H.S., A.M.S., J.H., R.A.F., J.M., M.L., E.J.E., A.H., V.T.C., P.D.D., and M.P. performed research; T.H., A.G., M.H.H., J.P., J.R., and L.F. contributed new reagents/analytic tools; P.J. analyzed data; and P.J., J.H.S., A.M.S., S.J.D., and D.K. wrote the paper.

The authors declare no conflict of interest.

This article is a PNAS Direct Submission.

¹P.J. and J.H.S. contributed equally to this work.

²To whom correspondence may be addressed. Email: x.xu@imperial.ac.uk, simon.davis@imm.ox.ac.uk, or dk10012@cam.ac.uk.

This article contains supporting information online at www.pnas.org/lookup/suppl/doi:10.1073/pnas.1513918113/-DCSupplemental.

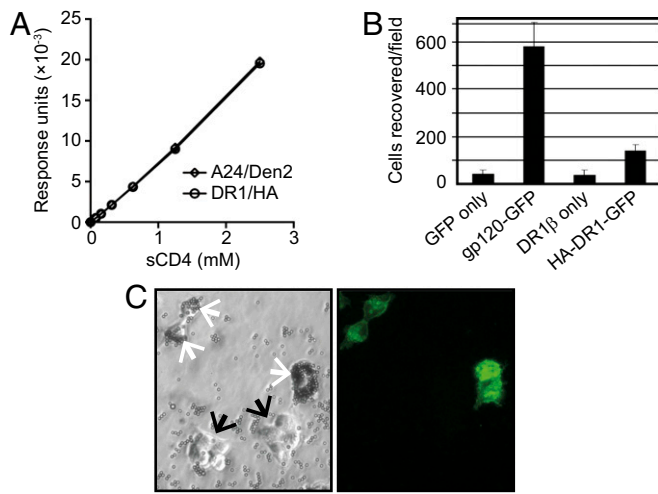


Fig. 1. The interaction of CD4 with pMHC II in solution is very weak. (A) SPR data showing the response when passing sCD4 over sensor surface presenting immobilized biotinylated pMHC II molecules (DR1/HA; ○), or pMHC I molecules (A24/Den2; ◇) as a control. (B) Number of isolated pMHC II (HA-DR1-GFP)-expressing HEK 293T cells that bound to biotinylated sCD4-coated beads. Error bars show ± one SEM. (C) A bright-field image of cells with bound sCD4-coated beads (Left); white and black arrows identify individual or clustered cells expressing or not expressing HA-DR1-GFP based on a corresponding fluorescence image (Right).

bonds had time to develop and reduced the risk of biasing the data toward cells with high avidity for CD4 (15).

Other 2D K_d measurements have been made, but only for systems where the average K_d is significantly lower than that of CD4/pMHC II binding (12, 13, 16, 17). Here, we use the method of Zhu et al. (16) to measure the 2D K_d for the CD4/pMHC II interaction, which proves to the best of our knowledge to be the weakest such interaction ever studied. The surface density of CD4 bound to pMHC II on the B cell, B , is related to the surface density of free CD4 in the SLB beneath the cell, F , by the Zhu-Golan expression

$$\frac{B}{F} = \frac{N_t \times f}{K_d \times S_{\text{cell}}} = \frac{B \times p}{K_d}, \quad [1]$$

where N_t and f are the number and mobile fraction of pMHC II molecules, respectively, S_{cell} is the surface area of the cell, and p is the ratio of the SLB/cell contact area to S_{cell} . Measurements were also made for rat CD2 and CD48 for comparison and as a test of the CD4/pMHC II results. Finally, we consider why CD4/pMHC II binding is so weak and develop a mathematical model to investigate how it could affect the stability of TCR/pMHC II complexes and affect rates of Lck recruitment and TCR phosphorylation. Our findings extend the known physical limits of functional protein interactions at the cell surface.

Results

Binding of Soluble CD4 to pMHC II. We first tried to directly measure the binding affinity of CD4 for pMHC II molecules in SPR-based assays. For this, soluble biotinylatable human CD4 (sCD4) was expressed in mammalian cells (18) (*Materials and Methods*). sCD4 bound stoichiometrically at distinct epitopes to two different mouse anti-human CD4 antibodies (ADP318 and RPA-T4; Fig. S1 A and B), and it also bound to HIV-1 gp120 (Fig. S1C), indicating that it was homogeneous and correctly folded. sCD4 was injected at different concentrations at 37 °C over a sensor surface presenting immobilized HLA-DRB1*01:01/DRA*01 (DR1) pMHC II bound with influenza HA peptide or HLA-A*24:02 (A24) pMHC I bound

with a Dengue peptide (Den2) as a negative control (Fig. 1A). The pMHC II proteins bound strongly to L243, a conformation-sensitive, pan anti-human DR antibody (Fig. S24), indicating that the pMHC II was functional. However, even at exceptionally high concentrations of sCD4 (up to 2.5 mM), no significant difference in response was detectable between the control and the pMHC II-containing flow cells (Fig. 1A). Injections at the highest concentration (2.5 mM) at 4 °C (to minimize dissociation) also gave no binding (Fig. S2B). These measurements were repeated with two other pMHC II, HLA-DRB1*15:01/DRA*01 (DR2) bound with MBP peptide and HLA-DRB1*04:01/DRA*01 (DR4) bound with EBV peptide, with the same outcome (Fig. S3).

To confirm that sCD4 could bind pMHC II we developed a multivalent binding assay. DR1, the beta chain of which was attached N-terminally to HA peptide and C-terminally to GFP (i.e., HA-DR1-GFP; Fig. S44), was expressed in HEK 293T cells. Biotinylated sCD4 (sCD4biot) tetramerized with phycoerythrin-labeled streptavidin (SA) bound strongly to HEK 293T cells expressing HIV-1 gp120-GFP, but not to cells expressing HA-DR1-GFP (Fig. S4B). sCD4biot avidity was then increased by attaching it to SA-coated magnetic beads (~50,000 sCD4biot per bead) and used to “pull down” HA-DR1-GFP-expressing cells (Fig. 1B; example bead-bound cells are shown in Fig. 1C). Three- to fourfold more cells expressing HA-DR1-GFP could be recovered than cells expressing the DR1β chain or GFP only (Fig. 1B), demonstrating binding of sCD4 to HA-DR1-GFP. However, this was only a quarter of the recoverable gp120-GFP-expressing cells (Fig. 1B), emphasizing the very low affinity of CD4/pMHC II binding. The interaction was sensitive to mutations of residues clustered in the pocket between the α2 and β2 domains used by affinity-matured CD4 to bind DR1 and DR4 (19), that is, β1148, βL158, αT90, and αL92 (Fig. 2, Fig. S4C and SI Text, *Mutation Analysis of the CD4 Binding Site of DR1*).

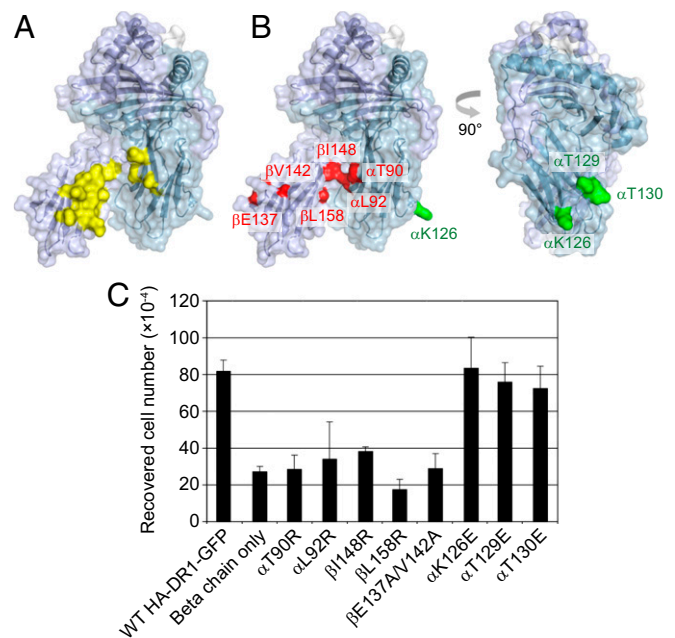


Fig. 2. The native CD4 binding site of pMHC II. (A) The surface of HLA-DR1 (PDB ID code 3S4S) is shown over a ribbon representation of its secondary structure (alpha chain in blue; beta in purple). The surface corresponding to residues that are buried by CD4 in the complex is highlighted in yellow. (B) Two orthogonal surface views showing residues whose mutation disrupts binding to CD4 (red), and residues whose mutation has no effect (green). (C) Histogram showing the numbers of cells recovered via the binding of CD4-coated magnetic beads, for each of the mutant proteins. Error bars show ± one SD.

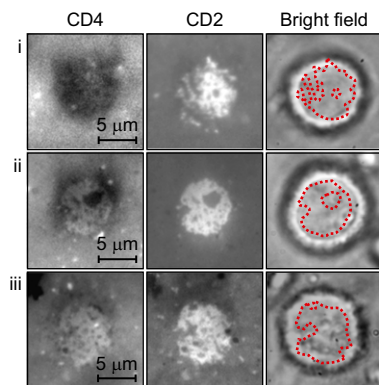


Fig. 3. Fluorescence images showing different degrees of accumulation of CD4 and CD2 beneath the B cell shown in the bright-field images to the right. The dashed line in the bright-field images shows the contour of the SLB/cell contact identified by CD2 accumulation. The numbering i to iii corresponds to different cases of CD4 accumulation in the SLB/cell contact.

Mutations of residues analogous to those in pMHC I that bind CD8, that is, β E137 and β V142, were disruptive, as noted previously (20), due perhaps to indirect effects on the structure of the pocket. Mutations of α K126, α T129, and α T130 at a second site proposed to allow CD4/pMHC II complex oligomerization (21) were without effect, however, implying that CD4 does not bind this region. Overall these data are consistent with native CD4 binding pMHC II at the single site identified in structures of cross-species and affinity-matured CD4/pMHC II complexes, and with binding being undetectable in SPR experiments due to the very low solution affinity of this interaction.

Binding of B Cells to CD4 in Lipid Bilayers. SLBs containing different amounts of Alexa Fluor 647-labeled, lipid-anchored CD4 (400–4,000 molecules/ μm^2) were used to investigate CD4/pMHC II binding at the B-cell surface at room temperature (22 °C). Raji B cells were added above the SLB and allowed to bind to the proteins in the SLB. To ensure firm contact, and to position the cell surface at physiologically relevant distances (22), \sim 400 molecules/ μm^2 of Alexa Fluor 488-labeled, lipid-anchored CD2 was incorporated in the SLB. *Movie S1* shows B cells settling on an SLB containing 900 molecules/ μm^2 of CD4 and 400 molecules/ μm^2 of CD2.

Three types of SLB/B-cell contacts formed (Fig. 3). Clear increases in CD2 fluorescence beneath the cells are observed in all three cases but, for case i, the CD4 intensity decreases compared with outside the cell, whereas in cases ii and iii it increases slightly (see also Fig. S5). The distribution of cases is i, $22 \pm 15\%$; ii, $52 \pm 12\%$; and iii, $26 \pm 11\%$ (mean value \pm one SD from 12 experiments), where, from Fig. S5, case i is defined as cells to the left of the kink in the fitted curve and cases ii and iii as cells on the lower and upper half of the slope, respectively. In case ii it is also seen that under the cell, but outside the contact area given by the CD2 image (dotted contour in the bright-field image, Fig. 3), the intensity is significantly lower compared with outside the cell (see also *SI Text, Kinetic Binding Theory*). The reason for this is that unbound CD4 is excluded from the cell–cell contact. Case i corresponds to an SLB/B-cell contact where no amount of CD4 binding is discernible. This behavior is not limited to CD4 binding to B cells: CD4 depletion was observed in SLB contacts formed by pMHC II nonexpressing Jurkat cells (Fig. S6A), and rat CD2 added to the SLBs, which does not bind human B cells, was depleted at B-cell contacts (Fig. S6B). However, in these cases depletion only was observed, and not accumulation as observed for the SLB with CD4/B-cell contacts (see cases ii and iii in Fig. 3), indicating that CD4/pMHC II binding was being measured. Ligand depletion observed elsewhere has been attributed to steric

crowding at the contact (17). This can significantly affect the analysis of binding affinity using Eq. 1 if not corrected for, especially when $B/F < 1$ (16, 17) (see *SI Materials and Methods, 2D Affinity* for details of how compensation was made).

Zhu–Golan Analysis of CD4/pMHC II Binding. The amount of CD4 accumulation under different cells on a given SLB varied considerably (Fig. S5), with the SD of B/F for each experiment being \sim 70% of the mean. However, the mean value from different sets of experiments under similar conditions has a much smaller spread and is fairly reproducible (Fig. 4). The variation therefore results from differences between the cells and their CD4 avidity rather than measurement uncertainty. Plotting the mean value of B/F from each SLB resulted in the data shown in Fig. 4 for CD4/pMHC II binding and for rat CD2 (35–1,600 molecules/ μm^2) binding to rat CD48 [either WT or a weakly-binding mutant Q40R (23)]. For the latter experiments CD48-transfected Jurkat T cells were used and \sim 100 molecules/ μm^2 of human CD58 was added to the SLBs to position the cells (Fig. S6 C and D).

The experimental data were fitted to Eq. 1 with values of N_t and S_{cell} determined as described in *Materials and Methods* (see Table 1 for values), assuming a mobile fraction of $f = 1$. The only free parameter to fit is then K_d . This gave the following 2D K_d values: 4,800 molecules/ μm^2 for CD4/pMHC II (see also *SI Text, Accuracy of the CD4/pMHC II 2D K_d*), 38 molecules/ μm^2 for CD2/CD48 (WT), and 380 molecules/ μm^2 for CD2/CD48 (Q40R). To validate the analysis we also analyzed the rat CD2/CD48 (WT) data using the standard Zhu–Golan method, where the slope of the data in Fig. 4 is used to determine K_d without knowing N_t , f , and S_{cell} (16). The observation that the two values were the same (38 molecules/ μm^2) indicated that our method of analysis was approximately valid, at least for the rat CD2/CD48 case. We did not use the Zhu–Golan analysis for all datasets because using the slope to determine the K_d value is less accurate for the weaker interactions, because the slow change in B/F vs. $B \times p$ is less than, or comparable to, the accuracy of the measurements for those cases. This is less of a problem when fixing N_t , f , and S_{cell} , which gives more accurate values for K_d assuming that the error in choosing N_t , f , and S_{cell} is not too large.

The 2D K_d value for WT rat CD2/CD48 binding is similar in magnitude, but slightly smaller, than previous measurements (15). The 2D K_d value for the weak-binding Q40R mutant is 10-fold larger than that for the WT, similar to the ratio in the 3D K_d measurements (Table 1). These interactions are weak compared with many other protein interactions between T cells and APCs, as illustrated also by their relatively large 3D K_d values. However, the CD4/pMHC II 2D K_d at 5,000 molecules/ μm^2 is one to two orders

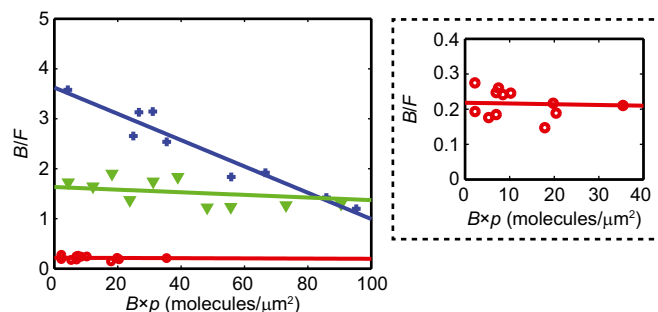


Fig. 4. (Left) Zhu–Golan curves showing the relative accumulation of ligands for three different protein-pair interactions: rat CD2/CD48 (WT; +), rat CD2/CD48 (Q40R; ▼), and CD4/pMHC II (○). The solid lines are linear fits to Eq. 1, with $N_t \times f$ and S_{cell} fixed, yielding K_d s for the different interactions. (Right) The spread of CD4/pMHC II data across a smaller scale.

Table 1. Values for the 2D K_d analysis and corresponding solution (3D) K_d values

Quantity	CD4/pMHC II [†]	CD2/CD48 (WT)	CD2/CD48 (Q40R)
N_t	570,000 ± 180,000 [‡]	95,000 ± 12,000	310,000 ± 50,000
S_{cell}	550 ± 70 μm ²	690 ± 50 μm ²	500 ± 80 μm ²
2D K_d	4,800 molecules/μm ²	38 molecules/μm ²	380 molecules/μm ²
3D K_d	>2.5 mM	37 μM	440 μM

[†]Protein in the SLB/protein in the contacting cell.

[‡]Values are presented as mean ± one SD.

of magnitude larger compared with these interactions, three orders of magnitude larger than that for human CD2/CD58 binding (17), and two to three orders of magnitude larger than that for TCR/pMHC interactions (13, 24). The 3D K_d values for the latter interactions is ~10 μM (10, 13, 24, 25), so it can be expected that the 3D K_d for CD4/pMHC II binding should, similar to the 2D K_d , be two to three orders of magnitude larger than this value. This is in agreement with a lower limit of 2.5 mM for the 3D K_d of the CD4/pMHC II interaction measured here using SPR, although extrinsic factors such as the average distance between the two cell surfaces could in principle significantly affect binding in 2D vs. 3D. Measurements of the CD4/pMHC II 2D K_d were also made at 37 °C. The B/F ratios from different SLBs were, within the accuracy of the experiments, similar to those at room temperature.

A delimited area of the SLB/B-cell contact was bleached and recovery studied to investigate the dynamic behavior of the CD4/pMHC II interaction (Fig. S7). The fluorescence from free and bound CD4 almost completely recovered within 2 min, indicating that the amount of trapped CD4 in the contact is small compared with the density of mobile molecules. From a fit of the recovery data (Fig. S7B) an average diffusivity of $D = 0.16 \pm 0.06 \mu\text{m}^2/\text{s}$ ($n = 4$) was obtained for CD4 in the contact. This value is 10 times smaller than that for free CD4 outside the contact ($1.8 \pm 0.2 \mu\text{m}^2/\text{s}$; $n = 4$), most likely caused by a higher net drag on the protein in the contact, rather than specific CD4 binding events (see *SI Text, Measure of CD4 Turnover Using Photobleaching* for details).

Modeling of the Effects of CD4 on TCR/pMHC II Stability and Phosphorylation Rate. Different mathematical expressions were derived to investigate how the very weak CD4/pMHC II interaction affects T-cell sensitivity and the stability of ternary TCR/pMHC II complexes.

Effect of CD4 on Lck recruitment to nonphosphorylated TCRs. CD4-associated Lck (CD4-Lck) can only phosphorylate the TCR complex when it is within a certain area, A , around the TCR/pMHC II. It can be assumed that Lck is within area A when CD4-Lck binds to pMHC II in a TCR/pMHC II pair, which means that bound CD4-Lck can phosphorylate the TCR/pMHC II complex an extra fraction R_t/K_c of the time (see *SI Text, Recruitment of CD4-Lck to Nonphosphorylated TCR/pMHC II* for details), where R_t is the density of CD4-Lck and K_c is the 2D K_d of the CD4/pMHC II interaction. This results in the following formula for the overall rate of TCR phosphorylation by CD4-Lck, for which the second term is due to Lck recruitment:

$$k_{p, \text{CD4-Lck/TCR}} = k_{p, \text{Lck/TCR}}(1 + \sigma/K_c), \quad [2]$$

where $k_{p, \text{CD4-Lck/TCR}}$ and $k_{p, \text{Lck/TCR}}$ are the rates of TCR phosphorylation by CD4-Lck and Lck, respectively, and $\sigma = 1/A$ is an effective local concentration corresponding to one molecule within area A . The actual size of A has not been experimentally determined but is estimated to be of the order of 100 nm², corresponding to $\sigma = 10,000 \text{ molecules}/\mu\text{m}^2$ (8, 9, 26). This is also comparable to the area occupied by Lck in the CD4-Lck/TCR/pMHC II complex (19). With $K_c = 5,000 \text{ molecules}/\mu\text{m}^2$, $k_{p, \text{CD4-Lck/TCR}}$ is a factor of three larger than $k_{p, \text{Lck/TCR}}$.

Effect of CD4 on the stability and phosphorylation of ternary CD4-Lck/phosphorylated TCR/pMHC II complexes. Following TCR phosphorylation CD4-Lck can bind phosphorylated tyrosines in the TCR complex (27). To investigate how this can affect the recruitment of Lck and the stability of TCR/pMHC II in the ternary complex, we developed a mathematical model describing the equilibrium distribution of CD4-Lck, pMHC II, and phosphorylated TCR (TCR-P) in different binding states (Fig. S8 and *SI Text, Equilibrium Models to Describe the Distribution of CD4-Lck, TCR-P, and pMHC II*). The number of TCR-P is assumed to be low early in T-cell responses, such that most CD4-Lck molecules are not bound to TCR-P. The increase in effective affinity of TCR for pMHC II, $1/K_{\text{eff}}$, in the presence of CD4 can, under these conditions, be shown to be (see *SI Text, Equilibrium Models to Describe the Distribution of CD4-Lck, TCR-P, and pMHC II* for details)

$$\frac{1/K_{\text{eff}}}{1/K} = \left(1 + \frac{R_t}{K_1} + \frac{R_t\sigma}{K_c K_1} + \frac{R_t K}{K_c K_1}\right) \times \left(1 + \frac{R_t}{K_1}\right)^{-1} \approx 1 + \frac{R_t(\sigma + K)}{K_c K_1}, \quad [3]$$

where K_1 and K are the 2D K_d values for binding of CD4-Lck to TCR-P and TCR-P to pMHC II, respectively. The parameter σ corresponds again to the local concentration of bound molecules in the complex (see also Eq. 2), which for simplicity was set to be equal for all three interactions. It has been assumed in Eq. 3 that both the concentration of pMHC II and R_t are significantly lower than K_c . The rightmost expression is approximately valid when $R_t/K_1 < 1$. Inserting $\sigma = 10,000 \text{ molecules}/\mu\text{m}^2$, $K_c = 5,000 \text{ molecules}/\mu\text{m}^2$, and $R_t/K_1 = 0.01\text{--}0.1$ (see *SI Text, Equilibrium Models to Describe the Distribution of CD4-Lck, TCR-P, and pMHC II* for details on how R_t/K_1 is estimated) into Eq. 3 gives an apparent affinity increase of 2–20%, respectively, when $K \ll \sigma$. CD4 will thus only modestly affect the stability of the TCR/pMHC II interaction under these conditions.

Using the same assumptions and parameter values the increase in recruitment of CD4-Lck to TCR-P due to CD4/pMHC II binding can also be estimated. For $K_1 = 250 \text{ molecules}/\mu\text{m}^2$ (28), the fraction of CD4-Lck-associated TCR-P/pMHC II increases by 2.6- and 3.0-fold for $R_t/K_1 = 0.1$ and $R_t/K_1 = 0.01$, respectively (see Eq. S18). The subsequent phosphorylation of the TCR complex, as well as phosphorylation of recruited ZAP70, will therefore also be increased by approximately threefold (see Eq. S17). It should finally be noted that, from Eq. S17 and Eq. 2 this phosphorylation rate ($k_{p, \text{CD4-Lck/TCR-P}}$) is 30–40 times larger (depending on the value for R_t/K_1) than the initial rate of phosphorylation, that is, of the unphosphorylated receptor ($k_{p, \text{CD4-Lck/TCR}}$ in Eq. 2).

Discussion

The binding of CD4 to pMHC II is remarkably weak compared with the interactions of other molecules expressed by T cells and APCs. Here, sCD4 monomers failed to bind pMHC II at concentrations as high as 2.5 mM, setting a new lower limit for the solution K_d . To confirm that this measurement was reliable we established a binding assay wherein, in a highly multivalent form, sCD4 binding to cell-expressed pMHC II could be detected.

Using this assay we confirmed that for native CD4 the binding site on pMHC II corresponds to that suggested by crystal structures of cross-species and affinity-matured CD4/pMHC II complexes (5, 6). It can therefore be assumed that native CD4 forms the same “v-shaped” complex that affinity-matured CD4 forms with TCR/pMHC II, wherein contact with the TCR is seemingly precluded (19). It thus seems very unlikely that the ternary CD4/pMHC II/TCR interaction is stabilized by direct interactions between the extracellular domains of CD4 and the TCR.

To characterize binding in 2D approximating the conditions at T-cell/APC contacts, we studied the interactions of B cells with SLBs containing human CD4 and used CD2 to initially anchor and then position the cell on the SLB at a physiologically relevant distance. Zhu–Golan analysis gave a 2D K_d of $\sim 5,000$ molecules/ μm^2 for the CD4/pMHC II interaction, to our knowledge the largest value ever reported for protein interactions at the cell surface. This value is two to three orders of magnitude larger than typical interactions between molecules expressed by T cells and APCs but is still specific because CD4 in SLBs did not interact with cells lacking pMHC II. Photobleaching measurements showed that CD4/pMHC II binding is reversible, and that the mobility of CD4 in the contact is more than 10-fold lower compared with outside the contact. Although the 2D off-rate (k_{off}) for the CD4/pMHC II interaction could not be determined in the present experiments, it can be estimated to be of the order of 250 s^{-1} (see *SI Text, Estimation of Kinetic Rate Constants* for details). With a 2D K_d value of $5,000$ molecules/ μm^2 this gives a 2D on-rate (k_{on}) of $0.05 \mu\text{m}^2 \text{ molecules}^{-1} \text{ s}^{-1}$, which is comparable to that measured for protein–protein interactions of higher affinity between T cells and APCs (13, 29). However, the k_{off} is orders of magnitude larger (12, 13, 29).

The 2D K_d value obtained here corresponds to the equilibrium value when two cells, or lipid bilayers with proteins, are held with their surfaces positioned relative to each other at a distance similar to that in the synaptic contact between T cells and APCs. Other techniques involving, for instance, micropipettes to periodically bring cells containing the two proteins into contact (12, 30), have been used to study the binding kinetics of single bonds when the cells are not aligned. However, including stronger binding auxiliary molecules to align and position the contacting surface, such as rat CD2/CD48 in this work, would be problematic in pipette-based experiments because the binding kinetics of the auxiliary molecules would dominate the overall signal vs. that for the specific CD4/pMHC II interaction. The 2D K_d value obtained for the CD4/pMHC II interaction could be different when T cells contact APCs versus B cells contacting SLBs containing CD4 and CD2. However, the observation that the CD4/pMHC II interaction is orders of magnitude weaker than typical T-cell/APC protein interactions is expected to hold.

What are the implications of the very large dissociation constant, and how does CD4 so profoundly affect T-cell signaling? The important role of CD4 *in vivo* is believed to be the recruitment of Lck to the TCR (8, 9, 31). The recruited Lck would phosphorylate immunoreceptor tyrosine-based activation motifs constituting an early step of T-cell activation (8, 9). In agreement with this, Xu and Littman (27) found that T-cell responses were significantly reduced if CD4 could not bind pMHC II, and that this depended on CD4–Lck being able to bind phosphorylated tyrosines in the TCR. Huppa et al. (13) and Hong et al. (30) also recently showed that CD4 has a negligible effect on the affinity and lifetime of TCR/pMHC II complexes, indicating that the primary role of CD4 is not TCR/pMHC II stabilization. To see whether our measured affinity of CD4 for pMHC II fits with these results we undertook numerical calculations to establish whether, in particular, (i) CD4 contributes to initial TCR phosphorylation (Fig. 5A) and (ii) how the CD4/pMHC II interaction affects the effective affinity of the TCR for pMHC II and the recruitment of Lck to previously phosphorylated TCRs (Fig. 5B).

The mathematical expressions showed that despite the very low affinity of CD4 for pMHC II it is sufficiently strong to

increase the rate of phosphorylation of both unphosphorylated and previously phosphorylated TCRs up to threefold due to the recruitment of Lck. However, the effective affinity of the TCR for pMHC II only increased marginally (2–20%) under the same conditions, in agreement with previous experimental observations (13, 30). This indicates that the decrease in T-cell sensitivity when CD4/pMHC II binding is blocked arises from a reduction in TCR phosphorylation by Lck, rather than from destabilization of TCR/pMHC II binding. It should, however, be noted that the increase in Lck recruitment of a factor of three is significantly less than the 10- to 100-fold decrease in sensitivity observed in antibody blocking experiments when calcium and IL-2 signaling are monitored (7, 32). A possible explanation for this is that the increase in phosphorylation is magnified by the exponential lifetime of the TCR/pMHC bond (26) as well as by the requirement for multiple triggering events to act cooperatively in producing calcium fluxes and downstream signaling (33). The derived expressions also showed that the phosphorylation of previously phosphorylated TCRs is significantly (30–40 times) faster than the phosphorylation of unphosphorylated TCRs. This results from CD4–Lck binding to TCR-P, explaining the observation by Xu and Littman (27) that T-cell responses are significantly reduced when Lck cannot bind to TCR-P. It also indicates that phosphorylation of the first tyrosine(s) in the TCR complex is rate-limiting for TCR phosphorylation.

It needs to be emphasized that these calculations are only approximations and their purpose is to illustrate how, even with the low affinity we have measured, CD4/pMHC II binding can augment T-cell signaling. However, it is also possible that CD4 function and signaling are rather more dependent on prior TCR/pMHC II engagement, because this facilitates CD4 recruitment. For example, the 2D K_d of the CD4/pMHC II interaction could be lower due to suppressed membrane fluctuations and/or optimal positioning of pMHC II for CD4 binding (34) (Fig. S9). Other processes, such as phosphorylation by tyrosine kinases not associated with CD4, might also affect initial signaling rates. It is furthermore possible that because the local concentration of CD4–Lck is increased in the immunological synapse (31), this could start to stabilize TCR-P/pMHC II in the synapse according to Eq. 3, which would also increase sensitivity. It is clear that more experiments are therefore needed to completely understand the role of CD4 in T-cell activation, but our data provide two key insights. First, the interaction of CD4 with pMHC II is very weak but measurable and specific, and second, at this low affinity, CD4 binding can enhance TCR phosphorylation without significantly stabilizing TCR/pMHC II binding. Too low a K_d for the CD4/pMHC II interaction would have detrimental effects on the discrimination of self from nonself peptides, whereas a too high K_d would result in too few interactions with pMHC II molecules for signaling to be enhanced via the delivery of CD4–Lck to the binary TCR/pMHC II complex.

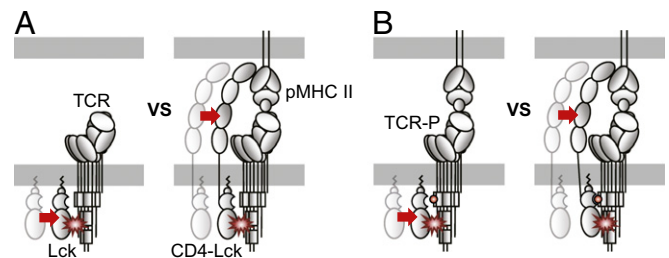


Fig. 5. The interaction between CD4 and pMHC II increases the phosphorylation rate of TCR but has less influence on the TCR/pMHC II stability. (A) Schematic illustrations showing how binding of CD4–Lck to pMHC II increases the rate of initial TCR phosphorylation. (B) Binding of CD4–Lck to TCR-P increases the rate of phosphorylation by recruitment of Lck but has only a modest effect on the effective affinity of the TCR/pMHC II complex.

Materials and Methods

The materials and methods used are summarized below; detailed information is given in [Supporting Information](#). Institutional review board approval was not required for use of the human cell lines or DNA constructs referred to.

Solution Affinity and Bead-Binding Experiments. sCD4 protein and soluble, biotinylatable forms of DR1/HA (residues 307–318:PKYVKQNTLKLK), DR2/MBP (residues 85–99:ENPVVHFVKKIVTPTR), DR4/EBV (residues 627–641: TGGVYHFVKKHVVHES), and A24/Den2 (residues 555–564:INADRRWCFC) were produced as described previously (35, 36). For testing for binding to sCD4, the biotinylated pMHC II was immobilized on Biacore streptavidin-coated chips at levels of 1,600 response units (RU) (DR1/HA), 1,750 RU (DR2/MBP), and 1,840 RU (DR4/EBV). A24/Den2, a kind gift of Tao Dong, University of Oxford, Oxford, was immobilized as a negative control at 1,600–1,900 RU. The affinities of WT and Q40R-mutated rat CD48 were measured as described previously (23).

For the bead-binding assay, HEK 293T cells were transfected with constructs encoding fluorescent HA-DR1-GFP or gp120-GFP as a control (see [SI Materials and Methods, 3D Affinity](#) for details). To generate CD4-coated beads 10 μ g biotinylated sCD4 protein was incubated with 6.7×10^6 magnetic streptavidin beads M-280 (DynaL Biotech). HEK 293T cells were transiently transfected by calcium phosphate precipitation with alpha and beta chain constructs to express WT or mutant HA-DR1-GFP molecules (Fig. S4) or gp120-GFP controls. Following magnetic “pull-down,” cells were either viewed by fluorescence microscopy and counted in duplicate microscope fields or absolute numbers of cells recovered were determined using a hemocytometer.

2D Affinity Measurements. An SLB consisting of 1-palmitoyl-2-oleoyl-*sn*-glycero-3-phosphocholine (POPC) from Avanti Polar Lipids with 5–10 wt % of 1,2-dioleoyl-*sn*-glycero-3-[(N-(5-amino-1-carboxypentyl)iminodiacetic acid)succinyl]

(nickel salt) (DGS-NTA) (Avanti Polar Lipids) was formed by vesicle fusion. After formation of the SLB the solution was exchanged with a protein mixture of either (i) polyhistidine-tagged human CD2 (labeled with Alexa Fluor 488) and human CD4 (labeled with Alexa Fluor 647) for the CD4/pMHC II measurements or (ii) polyhistidine-tagged rat CD2 (labeled with Alexa Fluor 488) and human CD58 (labeled with Alexa Fluor 647) for the CD2/CD48 measurements.

Raji B cells or Jurkat cells expressing either WT or weakly binding Q40R mutant CD48 were added to the protein-coupled SLBs and were allowed to settle for ~60 min before imaging. Number of proteins on the cell surface, N_b , was determined by flow cytometry and Quantibrite analysis with saturating concentrations of PE-conjugated monoclonal antibodies (see [SI Materials and Methods, 2D Affinity](#) for details).

Fluorescence imaging was performed in total internal reflection mode with simultaneous imaging of the sample at 488 nm and 647 nm (see [SI Materials and Methods, 2D Affinity](#) for details of the microscope setup). Images of ~50 cells were acquired for each SLB. SLB protein densities were calculated using fluorescence correlation spectroscopy and the images were analyzed as detailed in [SI Materials and Methods, 2D Affinity](#) to obtain BIF and $B \times p$. S_{cell} was obtained from a bright-field image of the cell. Photo-bleaching measurements were performed with the same microscopy setup as described in [SI Materials and Methods, 2D Affinity](#).

ACKNOWLEDGMENTS. We thank Professor P. A. van der Merwe and Dr. Marco Fritzsche for helpful comments on the manuscript and Dr. Hugh Reid for technical advice on pMHC II expression. This work was supported by the Wellcome Trust, the UK Medical Research Council, and the Swedish Research Council Grants 623-2014-6387 and 621-2014-3907 (to P.J.). O.D. is supported by the Sir Henry Dale Fellowship Grant 098363 jointly funded by the Wellcome Trust and the Royal Society.

- Singer A, Adoro S, Park J-H (2008) Lineage fate and intense debate: Myths, models and mechanisms of CD4- versus CD8-lineage choice. *Nat Rev Immunol* 8(10):788–801.
- Norment AM, Salter RD, Parham P, Engelhard VH, Littman DR (1988) Cell-cell adhesion mediated by CD8 and MHC class I molecules. *Nature* 336(6194):79–81.
- Doyle C, Strominger JL (1987) Interaction between CD4 and class II MHC molecules mediates cell adhesion. *Nature* 330(6145):256–259.
- Clayton LK, Sieh M, Pious DA, Reinherz EL (1989) Identification of human CD4 residues affecting class II MHC versus HIV-1 gp120 binding. *Nature* 339(6225):548–551.
- Wang XX, et al. (2011) Affinity maturation of human CD4 by yeast surface display and crystal structure of a CD4-HLA-DR1 complex. *Proc Natl Acad Sci USA* 108(38):15960–15965.
- Wang JH, et al. (2001) Crystal structure of the human CD4 N-terminal two-domain fragment complexed to a class II MHC molecule. *Proc Natl Acad Sci USA* 98(19):10799–10804.
- Irvine DJ, Purbhoo MA, Krosgaard M, Davis MM (2002) Direct observation of ligand recognition by T cells. *Nature* 419(6909):845–849.
- Artyomov MN, Lis M, Devadas S, Davis MM, Chakraborty AK (2010) CD4 and CD8 binding to MHC molecules primarily acts to enhance Lck delivery. *Proc Natl Acad Sci USA* 107(39):16916–16921.
- Stepanek O, et al. (2014) Coreceptor scanning by the T cell receptor provides a mechanism for T cell tolerance. *Cell* 159(2):333–345.
- van der Merwe PA, Davis SJ (2003) Molecular interactions mediating T cell antigen recognition. *Annu Rev Immunol* 21:659–684.
- Davis SJ, et al. (2003) The nature of molecular recognition by T cells. *Nat Immunol* 4(3):217–224.
- Huang J, et al. (2010) The kinetics of two-dimensional TCR and pMHC interactions determine T-cell responsiveness. *Nature* 464(7290):932–936.
- Hupp JB, et al. (2010) TCR-peptide-MHC interactions in situ show accelerated kinetics and increased affinity. *Nature* 463(7283):963–967.
- Wu Y, Vendome J, Shapiro L, Ben-Shaul A, Honig B (2011) Transforming binding affinities from three dimensions to two with application to cadherin clustering. *Nature* 475(7357):510–513.
- Dustin ML, et al. (1997) Low affinity interaction of human or rat T cell adhesion molecule CD2 with its ligand aligns adhering membranes to achieve high physiological affinity. *J Biol Chem* 272(49):30889–30898.
- Zhu D-M, Dustin ML, Cairo CW, Golan DE (2007) Analysis of two-dimensional dissociation constant of laterally mobile cell adhesion molecules. *Biophys J* 92(3):1022–1034.
- Dustin ML (2009) Supported bilayers at the vanguard of immune cell activation studies. *J Struct Biol* 168(1):152–160.
- Davis SJ, et al. (1992) Antibody and HIV-1 gp120 recognition of CD4 undermines the concept of mimicry between antibodies and receptors. *Nature* 358(6381):76–79.
- Yin Y, Wang XX, Mariuzza RA (2012) Crystal structure of a complete ternary complex of T-cell receptor, peptide-MHC, and CD4. *Proc Natl Acad Sci USA* 109(14):5405–5410.
- König R, Huang LY, Germain RN (1992) MHC class II interaction with CD4 mediated by a region analogous to the MHC class I binding site for CD8. *Nature* 356(6372):796–798.
- König R, Shen X, Germain RN (1995) Involvement of both major histocompatibility complex class II alpha and beta chains in CD4 function indicates a role for ordered oligomerization in T cell activation. *J Exp Med* 182(3):779–787.
- James JR, Vale RD (2012) Biophysical mechanism of T-cell receptor triggering in a reconstituted system. *Nature* 487(7405):64–69.
- Evans EJ, et al. (2006) Crystal structure and binding properties of the CD2 and CD244 (2B4)-binding protein, CD48. *J Biol Chem* 281(39):29309–29320.
- Grakoui A, et al. (1999) The immunological synapse: A molecular machine controlling T cell activation. *Science* 285(5425):221–227.
- Rosjohn J, et al. (2015) T cell antigen receptor recognition of antigen-presenting molecules. *Annu Rev Immunol* 33(1):169–200.
- Dushek O, van der Merwe PA (2014) An induced rebinding model of antigen discrimination. *Trends Immunol* 35(4):153–158.
- Xu H, Littman DR (1993) A kinase-independent function of Lck in potentiating antigen-specific T cell activation. *Cell* 74(4):633–643.
- Hui E, Vale RD (2014) In vitro membrane reconstitution of the T-cell receptor proximal signaling network. *Nat Struct Mol Biol* 21(2):133–142.
- Tolentino TP, et al. (2008) Measuring diffusion and binding kinetics by contact area FRAP. *Biophys J* 95(2):920–930.
- Hong J, et al. (2015) Force-regulated in situ TCR-peptide-bound MHC class II kinetics determine functions of CD4+ T cells. *J Immunol* 195(8):3557–3564.
- Li Q-J, et al. (2004) CD4 enhances T cell sensitivity to antigen by coordinating Lck accumulation at the immunological synapse. *Nat Immunol* 5(8):791–799.
- Vidal K, Daniel C, Hill M, Littman DR, Allen PM (1999) Differential requirements for CD4 in TCR-ligand interactions. *J Immunol* 163(9):4811–4818.
- Huse M, et al. (2007) Spatial and temporal dynamics of T cell receptor signaling with a photoactivatable agonist. *Immunity* 27(1):76–88.
- Hu J, Lipowsky R, Weikl TR (2013) Binding constants of membrane-anchored receptors and ligands depend strongly on the nanoscale roughness of membranes. *Proc Natl Acad Sci USA* 110(38):15283–15288.
- Harkioliaki M, et al. (2009) T cell-mediated autoimmune disease due to low-affinity cross-reactivity to common microbial peptides. *Immunity* 30(3):348–357.
- Scaally SW, et al. (2013) A molecular basis for the association of the HLA-DRB1 locus, citrullination, and rheumatoid arthritis. *J Exp Med* 210(12):2569–2582.
- Dushek O, et al. (2008) Effects of intracellular calcium and actin cytoskeleton on TCR mobility measured by fluorescence recovery. *PLoS One* 3(12):e3913.
- Wu J, et al. (2008) A coupled diffusion-kinetics model for analysis of contact-area FRAP experiment. *Biophys J* 95(2):910–919.
- Sprague BL, Pego RL, Stavreva DA, McNally JG (2004) Analysis of binding reactions by fluorescence recovery after photobleaching. *Biophys J* 86(6):3473–3495.
- Altan-Bonnet G, Germain RN (2005) Modeling T cell antigen discrimination based on feedback control of digital ERK responses. *PLoS Biol* 3(11):e356.
- Kumar GS (2014) *Orban's Oral Histology & Embryology* (Elsevier Health Sciences, New Delhi), 13th Ed.
- Maroun CR, Julius M (1994) Distinct roles for CD4 and CD8 as co-receptors in T cell receptor signalling. *Eur J Immunol* 24(4):959–966.
- Nika K, et al. (2010) Constitutively active Lck kinase in T cells drives antigen receptor signal transduction. *Immunity* 32(6):766–777.
- Ballek O, Valečka J, Manning J, Filipp D (2015) The pool of preactivated Lck in the initiation of T-cell signaling: A critical re-evaluation of the Lck standby model. *Immunol Cell Biol* 93(4):384–395.
- Davis SJ, et al. (1990) High level expression in Chinese hamster ovary cells of soluble forms of CD4 T lymphocyte glycoprotein including glycosylation variants. *J Biol Chem* 265(18):10410–10418.
- Horrocks MH, et al. (2013) Single-molecule measurements of transient biomolecular complexes through microfluidic dilution. *Anal Chem* 85(14):6855–6859.
- Johansson B, Höök F, Klenerman D, Jönsson P (2014) Label-free measurements of the diffusivity of molecules in lipid membranes. *Chemphyschem* 15(3):486–491.